Topological phases for fermionic cold atoms on the Lieb lattice

N. Goldman*
Center for Nonlinear Phenomena and Complex Systems - Université Libre de Bruxelles (U.L.B.), Code Postal 231, Campus Plaine, B-1050 Brussels, Belgium

D. F. Urban
Physikalisches Institut, Albert-Ludwigs-Universität, D-79104 Freiburg, Germany

D. Bercioux
Freiburg Institute for Advanced Studies, Albert-Ludwigs-Universität, D-79104 Freiburg, Germany and Physikalisches Institut, Albert-Ludwigs-Universität, D-79104 Freiburg, Germany

(Received 24 January 2011; published 2 June 2011)

We investigate the properties of the Lieb lattice, that is, a face-centered square lattice, subjected to external gauge fields. We show that an Abelian gauge field leads to a peculiar quantum Hall effect, which is a consequence of the single Dirac cone and the flat band characterizing the energy spectrum. Then we explore the effects of an intrinsic spin-orbit term—a non-Abelian gauge field—and demonstrate the occurrence of the quantum spin Hall effect in this model. Besides, we obtain the relativistic Hamiltonian describing the Lieb lattice at low energy and derive the Landau levels in the presence of external Abelian and non-Abelian gauge fields. Finally, we describe concrete schemes for realizing these gauge fields with cold fermionic atoms trapped in an optical Lieb lattice. In particular, we provide a very efficient method to reproduce the intrinsic (Kane-Mele) spin-orbit term with assisted-tunneling schemes. Consequently, our model could be implemented in order to produce a variety of topological states with cold atoms.

DOI: 10.1103/PhysRevA.83.063601 PACS number(s): 03.75.Ss, 37.10.Jk, 05.30.Fk, 71.70.Di

I. INTRODUCTION

During the last decades, topology has influenced many fields of physics through the renewed description of various phenomena. In condensed-matter physics, topological invariants, known as Chern numbers, have played an important role in the description of the integer quantum Hall effect (IQHE) [1]. Here the quantized Hall conductivity of a two-dimensional (2D) electron system is expressed as a sum $\sigma_{\mathrm{H}} = R_{\mathrm{K}}^{-1} \sum_{E_n < E_{\mathrm{F}}} N_{\mathrm{Ch}}(E_n)$ of Chern numbers $N_{\mathrm{Ch}}(E_n)$ that are integers associated with the energy bands E_n [2,3]. In the latter expression, R_{K} is von Klitzing's constant and E_{F} denotes the Fermi energy assumed to lie inside a gap of the bulk energy spectrum. Furthermore, it has been proven that the sum of Chern numbers is expressing the number of gapless *edge states* located inside the bulk energy gaps. These edge states carry the current in the IQHE [4,5].

The breaking of time-reversal symmetry (TRS) due to external magnetic fields plays a crucial role for the topological interpretation of the IQHE [6]. Recently the discovery of the so-called quantum spin Hall effect (QSHE) has lightened a new path for the investigation of systems where TRS is preserved [7–12]. The QSHE manifests itself in insulating systems that show a nontrivial Z_2 index [7]. These *topological insulators* are characterized by the presence of *spin-filtered* edge states in the gaps of the bulk energy spectrum. Because of TRS invariance, the spin-up and spin-down states move in opposite directions along the edge of the system. As a consequence, the total charge current as well as the associated Chern numbers are zero [12,13]. Yet a spin-Chern number has been introduced in order to measure the spin transport [14] and to distinguish the Z_2 class of the system [15].

The interplay between the lattice topology and the QSHE has been the focus of various recent investigations. In particular, the QSHE has been studied for the Kagome [16,17], the Lieb and Perovskite [18], the honeycomb [7,19], the square [20,21], the $\mathcal{T}_3$ [22], the checkerboard [23], the pyrochlore [24], diamond [25] and the square-octogon [26] lattices.

In this context some lattice models are of particular interest as they show dispersionless energy bands. These *flat bands* correspond to a macroscopic number of degenerate localized states. Originally flat bands played a fundamental role in magnetism, as they were shown to accompany the occurrence of ferromagnetic ground states in multiband Hubbard models [27–29]. More recently the existence and the robustness of these special bands have been extensively studied in a vast family of frustrated hopping models [30,31] and for the case of electron localization due to magnetic fields and spin-orbit interactions [32]. Interestingly, singular touchings between flat and dispersive bands have been shown to be topologically protected by real-space loops [30]. On the face-centered square lattice, also known as Lieb lattice, a flat band touches two linearly dispersing bands, that is, the flat band intersects a single Dirac point, and the low-energy regime is described by a quasirelativistic equation for spin-1 fermions [33,34]. Finally, the existence of flat bands with nontrivial topological order has been demonstrated [64], contradicting the belief that nondispersive bands were associated with vanishing Chern numbers [31].

Nowadays, various lattices can be engineered using cold atoms trapped by electromagnetic fields [34–39]. In particular, the realization of topological states of matter with cold

*ngoldman@ulb.ac.be

fermionic atoms appears to be a realistic and attractive goal from the experimental point of view [20,21,40]. A significant advantage of these experiments is the full control of a wide range of system parameters as, for example, lattice geometry, interaction, and disorder. In these experiments engineered gauge fields allow us to mimic the effects of magnetic fields [41–43] or spin-orbit interactions (SOIs) [20,21,44–48]. These gauge fields can be generated by spatially varying laser or magnetic fields that modify particle hopping via nontrivial Berry's phases [49–51]. Recent experiments have implemented light-induced external gauge fields and reproduced the physics of charges subjected to electric or magnetic fields [41,42,52,53]. Moreover, with such a setup one expects to observe several fundamental phenomena including the Hofstadter butterfly [43,54], atomic analogs of the quantum Hall effects [55,56], relativistic physics [57,58], and vortex structures [41,59,60]. Optical-lattice setups also allow us to consider a generalization of the ongoing experiments, namely the implementation of non-Abelian gauge fields [46,61–63]. In particular, non-Abelian gauge fields acting on multilevel atomic systems could mimic SOI [44–46,48,64], paving the way to study the spin Hall [65] and quantum spin Hall effects [17,21]. Very recently a concrete proposal of an optical Lieb lattice for cold atoms has been presented [37]. In the later work, Apaja *et al.* have shown that a fermionic cloud expanding after the release of the harmonic trap should show clear signatures of the flat band's localized states.

Motivated by the possibility of engineering an optical Lieb lattice for cold fermionic atoms, we investigate the emergence of topological properties for various configurations of synthesized gauge fields. We first provide an original analysis of a peculiar IQHE, in the case where a uniform magnetic field is present in the Lieb lattice. We then explore the effects of an intrinsic spin-orbit term [7] and show how it leads to quantum spin Hall states. In this framework we extend the seminal work of Ref. [18] and derive an effective Hamiltonian describing the low-energy regime. This Weyl-like Hamiltonian leads to a three-component quantum equation that resembles the relativistic equation for spin-1 particles. Besides, we obtain the Landau levels in the presence of an external magnetic field and spin-orbit interaction. Finally, we discuss the optical-lattice realization of this Lieb system and propose realistic methods for creating Abelian (magnetic) and non-Abelian (spin-orbit) gauge fields. We show that the Lieb lattice is particularly suited to reproduce the intrinsic spin-orbit term introduced by Kane and Mele [7]. The latter, which involves complex spin-dependent *next*-nearest-neighbor hoppings, can be simply decomposed into nearest-neighbor hopping on a square sublattice. This elegant idea is a non-Abelian generalization of the method proposed in Ref. [40] for generating the Abelian Haldane-type gauge field.

II. THE LIEB LATTICE AND TOPOLOGICAL PHASES IN EXTERNAL FIELDS

We consider the face-centered square (Lieb) lattice which is shown in Fig. 1. This lattice has a unit cell characterized by three lattice sites, hereafter referred to as H, A, and B. Site H has four nearest-neighbors (NN), namely two A and two B sites. On the contrary the A and B sites have only two

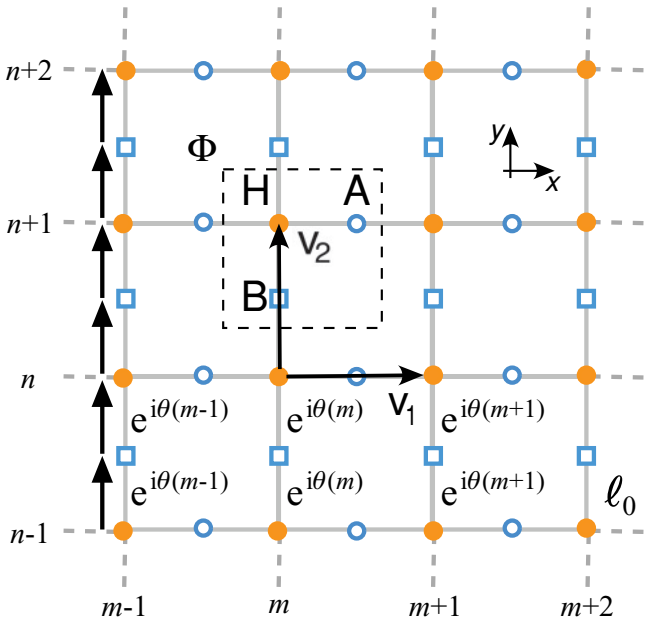

FIG. 1. (Color online) The face-centered square lattice or Lieb lattice. The Peierls phases $e^{i\theta(m)}$ where $\theta(m) = \pi\Phi m$ are associated to a uniform magnetic flux per plaquette Φ and are indicated by vertical black arrows. We set $x = 2m\ell_0$ and $y = 2n\ell_0$.

NN H sites. The bulk properties of the Lieb lattice can be analyzed within a tight-binding (TB) approximation. In this limit the Hamiltonian of the system can be written as $\mathcal{H}_0 = t\sum_{\langle i,j\rangle\alpha} c^\dagger_{i\alpha}c_{j\alpha}$ with spin independent NN hopping amplitude t. Here $c^\dagger_{j\alpha}(c_{j\alpha})$ is the creation (annihilation) operator for a particle with spin direction α on the lattice site j. In absence of external fields the problem can be diagonalized exactly and the spectrum reads

$$\varepsilon_0(\boldsymbol{k}) = 0, \tag{1a}$$

$$\varepsilon_\pm(\boldsymbol{k}) = \pm t\sqrt{4 + 2\ \cos(\boldsymbol{v}_1\cdot\boldsymbol{k}) + 2\cos(\boldsymbol{v}_2\cdot\boldsymbol{k})}, \tag{1b}$$

where $\boldsymbol{k} = (k_x, k_y)$ and $\boldsymbol{v}_{1/2}$ are the lattice vectors (cf. Fig. 1). The bulk energy spectrum is shown in Fig. 2(a). It depicts two identical, electron-hole symmetric branches $\varepsilon_\pm$. Moreover, the Lieb lattice presents a unique nondispersive band at the charge neutrality point (CNP). This band is rooted in the lattice topology which allows for insulating states with finite wave function amplitudes on the A and B sites and vanishing amplitudes on H sites. This property also holds when hopping to higher-order neighbors is allowed. Note that the three bands touch at the center of the first Brillouin zone, which we set for simplicity at $\Gamma = \pi/2\ell_0(1,1)$. The resulting properties of carriers in proximity of the Γ point are investigated in Sec. III.

A. Uniform magnetic field and quantum Hall phases

We now study the effects of a uniform magnetic field $\boldsymbol{B} = B\hat{z}$ on the spectral and transport properties of the Lieb lattice. We consider the Landau gauge

$$\boldsymbol{A} = (0, Bx, 0) = \left(0, \frac{\pi\Phi m}{\ell_0}, 0\right), \tag{2}$$

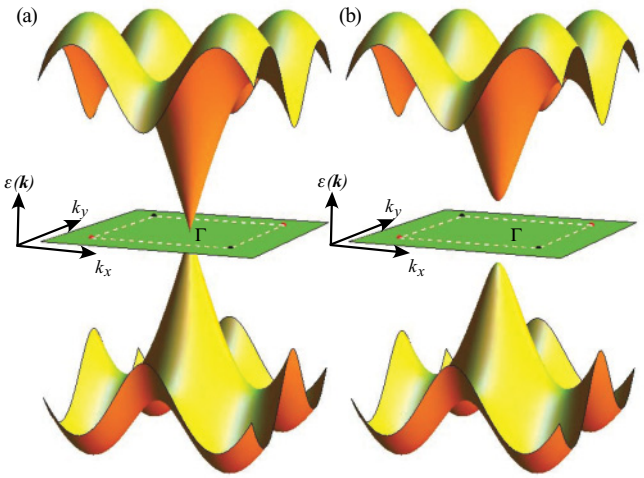

FIG. 2. (Color online) Energy spectrum of the Lieb lattice as a function of the momentum $\boldsymbol{k} = (k_x, k_y)$. The dashed lines delimit the first Brillouin zone. (a) Spectrum without external fields. (b) Energy spectrum in the presence of spin-orbit interaction $t_{\mathrm{SO}} = 0.1\,t$.

where $\Phi = \Phi_0^{-1} \int_{\square} \boldsymbol{B} \cdot \mathrm{d}\boldsymbol{S}$ is the number of magnetic flux quanta Φ_0 per plaquette and $x = 2m\ell_0$. Hereafter we use the notation (m,n,ζ), with $\zeta = \{\mathrm{A},\mathrm{B},\mathrm{H}\}$, to label the lattice sites. The gauge field $\boldsymbol{A}$ modifies the hopping along the y direction through x-dependent Peierls phases $t \to t\mathrm{e}^{\mathrm{i}\theta(m)}$, where the phase reads

$$\theta(m) = \int_{(m,n,\mathrm{H})}^{(m,n+1,\mathrm{B})} \boldsymbol{A} \cdot \mathrm{d}\boldsymbol{l} = \int_{(m,n,\mathrm{B})}^{(m,n,\mathrm{H})} \boldsymbol{A} \cdot \mathrm{d}\boldsymbol{l} = \pi \Phi m \quad (3)$$

(as illustrated in Fig. 1). Here the integrations are performed along the links connecting the neighboring B and H sites.

Setting $\Phi = p/q$, where p and q are mutually prime integers, the system becomes q periodic along the x direction. By considering periodic boundary conditions, it is possible to diagonalize the resulting $3q \times 3q$ spectral problem. This leads to the fractal energy spectrum shown in Fig. 3. As a function of the flux Φ the allowed energies depict two Hofstadter butterflies separated by a flat band at $E = 0$ [67]. This specific band is reminiscent of the flat band obtained at zero magnetic field.

The fractal energy spectrum of lattices subjected to uniform magnetic fields are intimately related to the IQHE [69,70]. When the Fermi energy E_{F} is located in a spectral gap, the Hall transverse conductivity of the system is quantized. This relation is supported by a Diophantine equation [71] which expresses the quantized Hall conductivity in terms of the magnetic flux and the position of the gap: In the rth gap the Hall conductivity is given by $\sigma_{xy} = (e^2/h)t_r$, where the integers (t_r, s_r) satisfy

$$r = pt_r + qs_r. \quad (4)$$

In general, the solutions (t_r, s_r) are not unique and additional criteria are needed in order to find quantized values of the Hall conductivity [71]. The integer t_r also has a topological

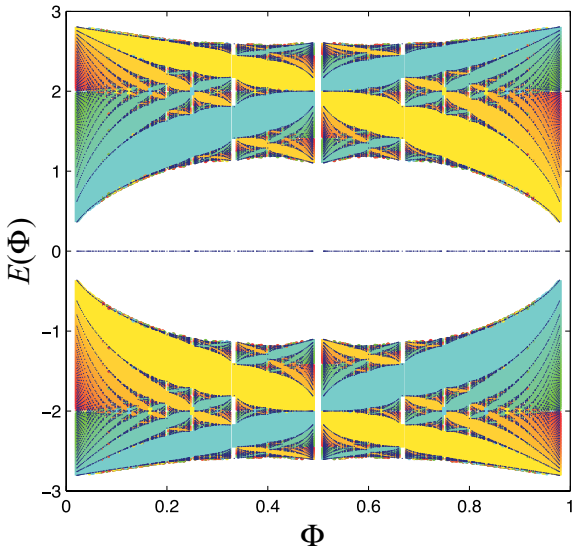

FIG. 3. (Color online) Spectrum $E = E(\Phi)$ and phase diagram for $\Phi = p/q$ with $q < 47$. The eigenvalues are dark blue dots forming two successive butterflies. Gaps are filled with cold (warm) colors according to the related positive (negative) values of the quantized conductivity σ_{xy}. The white gaps located around $E = 0$ correspond to $\sigma_{xy} = 0$. Note that the flat band at $E = 0$ is robust within the whole range $0 < \Phi < 1$.

interpretation, since it represents the sum of Chern numbers characterizing the bands below the Fermi energy E_{F}:

$$t_r = -\sum_{E_\lambda < E_{\mathrm{F}}} N_{\mathrm{Ch}}(E_\lambda). \quad (5)$$

In order to investigate the quantum Hall phases in the Lieb lattice, we have numerically evaluated the Chern numbers $N_{\mathrm{Ch}}(E_\lambda)$ using the method of Ref. [72]. We have verified that the integer t_r satisfies the Diophantine equation with the specific condition $|t_r| \leqslant q/2$ [71]. The full phase diagram describing the integer quantum Hall effect for the Lieb lattice is drawn in Fig. 3. It represents the infinitely many quantum Hall phases characterized by the quantized transport coefficient $\sigma_{xy} = (e^2/h)t_r$ inside the spectral gaps. The different positive (negative) values of the Hall conductivity are designated by cold (warm) colors.

To identify the Hall plateaus stemming from the uniform magnetic field, we represent the Hall conductivity $\sigma_{xy}(E_{\mathrm{F}})$ as a function of the Fermi energy in the low-flux regime $\Phi \ll 1$ (cf. Fig. 4). In this regime the quantized conductivity evolves monotonically but suddenly changes sign around the van Hove singularities (VHS) [73] located at $E = \pm 2\,t$ (see the alternation of cold and warm colors in Figs. 3 and 4). Note that the gaps surrounding the topological flat band at $E = 0$ correspond to normal band insulators with vanishing conductivity $\sigma_{xy} = 0$ for all values of the flux Φ. This is a consequence of the flat band's vanishing Chern number [31]. Most importantly, we observe that the Hall sequence presented in Fig. 4 shows steps of $\Delta\sigma_{xy} = (e^2/h)$. It is interesting to compare the latter result with the Hall sequences obtained for the $\mathcal{T}_3$ and honeycomb lattices [22,73] which are characterized by steps of $\Delta\sigma_{xy} = 2(e^2/h)$ between the VHS. This major difference [74] is due to the fact that the Lieb lattice is

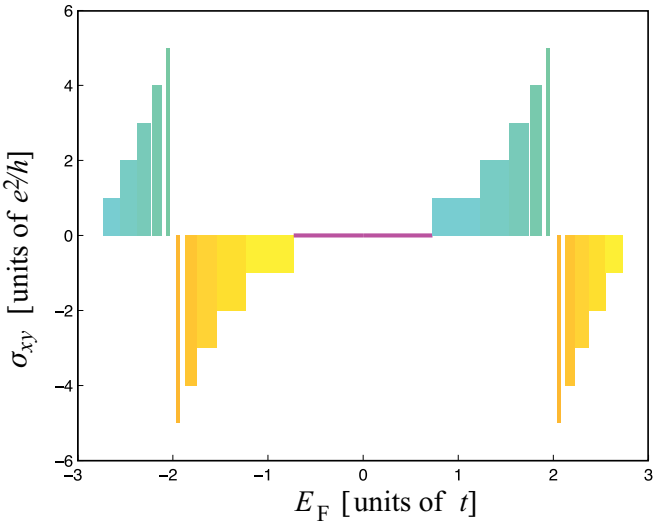

FIG. 4. (Color online) Hall conductivity $\sigma_{xy}(E_F)$ as a function of the Fermi energy for $\Phi = 1/11$. Cold (warm) colors correspond to positive (negative) values of the quantized conductivity, while the central plateau at $\sigma_{xy} = 0$ is represented in magenta.

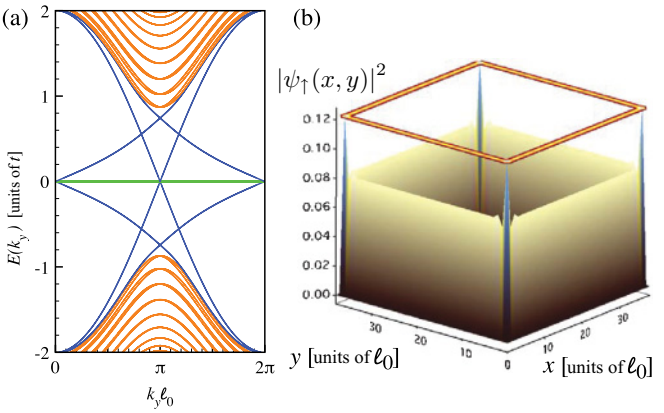

FIG. 5. (Color online) (a) Energy spectrum $E = E(k_y)$ in the cylinder geometry with $t_{SO} = 0.2t$. The bulk gap is traversed by gapless edge states (i.e., helical states). The flat band at $E = 0$ is highlighted by a green horizontal line. (b) Edge-states amplitude $|\psi_\uparrow(x,y)|^2$ for the open Lieb lattice with 39×39 sites, straight edges, and $t_{SO} = 0.5t$. This localized eigenstate satisfies $H\psi_\lambda(x,y) = E_\lambda\psi_\lambda(x,y)$ and corresponds to the energy $E_\lambda = 0.5t$ which lies within the gap.

characterized by a *single* relativistic cone, whereas the $\mathcal{T}_3$ and honeycomb lattices display *two* cones.

B. Spin-orbit interaction and quantum spin Hall phases

In this section we study the effects of spin-orbit interactions (SOIs) on the properties of the Lieb lattice. Specifically, we introduce an intrinsic SOI term in the TB Hamiltonian, in analogy with the model of Kane and Mele for graphene [6–8,18,22,75]. This term is modeled via a spin-dependent next-nearest-neighbor (NNN) hopping term

$$\mathcal{H}_{SO} = it_{SO}\sum_{\alpha\beta}\sum_{\langle\langle k,l\rangle\rangle} c^\dagger_{k,\alpha}(\mathbf{d}_i \times \mathbf{d}_j)\cdot\boldsymbol{\sigma}_{\alpha\beta}\, c_{l,\beta}. \tag{6}$$

The $\boldsymbol{\sigma}_{\alpha\beta}$ are matrix elements of the Pauli-matrices $\boldsymbol{\sigma}$ with respect to the final and initial spin states α and β and $\mathbf{d}_i$ and $\mathbf{d}_j$ are the two displacement vectors of the NNN hopping process connecting sites k and l. Since in 2D lattices hopping is naturally restricted to in-plane processes, the SOI is effectively proportional to σ_z. Because of the unequal connectivity of A or B and H sites, the term (6) effectively induces hopping between A and B sites only, that is, other NNN-hopping processes cancel. The spectrum is obtained by exact diagonalization [18] and reads

$$\varepsilon_0^{(SO)}(\boldsymbol{k}) = 0, \tag{7a}$$

$$\varepsilon_\pm^{(SO)}(\boldsymbol{k}) = 2\{\, t^2[\cos^2(\boldsymbol{v}_1\cdot\boldsymbol{k}) + \cos^2(\boldsymbol{v}_2\cdot\boldsymbol{k})] + 4t_{SO}^2\sin^2(\boldsymbol{v}_1\cdot\boldsymbol{k})\sin^2(\boldsymbol{v}_2\cdot\boldsymbol{k})\}^{\frac{1}{2}}. \tag{7b}$$

The bulk energy spectrum is shown in Fig. 2(b) for $t_{SO} = 0.1\,t$. Due to its topological origin the nondispersive band at $E = 0$ is not affected by SOI. However, this term opens two bulk energy gaps $\Delta_{gap} = 4\,t_{SO}$ between the nondispersive and the electron and hole branches, respectively.

The SOI has dramatic consequences on the transport properties of the Lieb lattice: as shown by Weeks and Franz, the gap Δ_{gap} allows for a topological insulating phase [18]. The latter is characterized by a robust spin transport along the edges of the system. This quantum spin Hall phase, induced by the intrinsic (Kane-Mele-type) spin-orbit term (6), can thus be directly visualized when studying a finite piece of the lattice, that is, by considering its edges.

A standard method consists of diagonalizing the TB Hamiltonian with periodic boundary conditions imposed along one of the spatial directions. This abstract cylinder contains two edges and already allows us to demonstrate the existence of helical edge states induced by the SOI. The corresponding energy spectrum [cf. Fig. 5(a)] depicts several edge-state channels: for each energy value within the bulk energy gap there exists a single time-reversed (or Kramers) pair of eigenstates localized on each edge of the lattice. The conservation of TRS prevents the mixing of these couple of states by small external perturbations and scattering from disorder [7,8].

The helical edge states characterizing the QSH phase are topologically protected against external perturbations. Their property can be quantified by looking at the Z_2-index ν [7]. This topological invariant characterizes the eigenstates defined in the bulk. It is defined on a 2-torus, in direct analogy with the Chern numbers introduced in the quantum Hall effect. Following Ref. [18], we have calculated this Z_2-index ν using the inversion symmetry of the lattice [25]. We obtain that SOI opens a spectral gap characterized by the index $\nu = 1$, therefore classifying the Lieb lattice as a quantum spin Hall insulator.

In the absence of spin-mixing perturbations, the Z_2 index is related to the spin Chern number n_σ [14,15] through the simple relation $\nu = n_\sigma \bmod 2$, where $n_\sigma = (N_\uparrow - N_\downarrow)/2$ and $N_{\uparrow,\downarrow}$ represent the Chern numbers associated with the individual spins. Using the numerical method of Ref. [72], we have obtained $n_\sigma = 1$ in agreement with the above result.

It is interesting to extend the analysis above by considering the more realistic open geometry, that is, a finite piece of Lieb lattice, thus characterized by a unique edge. We have solved the TB problem for a Lieb lattice of 39×39 sites with

realistic straight edges. This yields a discrete energy spectrum extending in the range $E \in [-2.8t, 2.8t]$. In the vicinity of the CNP, within a range corresponding to $\Delta_{\rm gap} = 4\ t_{\rm SO}$, the eigenvalues correspond to eigenstates that are localized at the edge of the system. This result is illustrated in Fig. 5(b), where the amplitude $|\psi_\uparrow(x,y)|^2$ is drawn for a particular edge state at $E = 0.5t$. Note that this coincides with $|\psi_\downarrow(x,y)|^2$. Using this geometry one can verify the helical property of these edge states by computing their associated current, which for spins σ is expressed as

$$j_x^\sigma(m,n) = -i\ell_0[\psi_\sigma^*(m+1,n)\mathcal{U}_x\,\psi_\sigma(m,n) + \sqrt{2}\psi_\sigma^*(m+1,n+1)\,\mathcal{D}\psi_\sigma(m,n) - \text{H.c.}], \quad (8)$$

$$j_y^\sigma(m,n) = -i\ell_0[\psi_\sigma^*(m,n+1)\mathcal{U}_y\,\psi_\sigma(m,n) + \sqrt{2}\psi_\sigma^*(m+1,n+1)\,\mathcal{D}\,\psi_\sigma(m,n) - \text{H.c.}]. \quad (9)$$

Here $\psi_\sigma(m,n) = (\psi_\sigma(m,n,\text{H}), \psi_\sigma(m,n,\text{A}), \psi_\sigma(m,n,\text{B}))$ and

$$\mathcal{U}_x = \begin{pmatrix} 0 & 0 & 0 \\ t\mathbb{I}_2 & 0 & -it_{\rm SO}\sigma \\ 0 & 0 & 0 \end{pmatrix}, \quad (10a)$$

$$\mathcal{U}_y = \begin{pmatrix} 0 & 0 & t\mathbb{I}_2 \\ 0 & 0 & -it_{\rm SO}\sigma, \\ 0 & 0 & 0 \end{pmatrix} \quad (10b)$$

$$\mathcal{D} = \begin{pmatrix} 0 & 0 & 0 \\ 0 & 0 & it_{\rm SO}\sigma. \\ 0 & 0 & 0 \end{pmatrix} \quad (10c)$$

We have verified that the currents $\boldsymbol{j}^\uparrow(m,n)$ and $\boldsymbol{j}^\downarrow(m,n)$ associated to the edge states yield two vector fields circulating along the edge in opposite directions.

III. LOW-ENERGY FERMIONS: THE QUASIRELATIVISTIC REGIME

In this section we focus on the properties of the Lieb lattice for noninteracting fermions at low energy, that is, close to the CNP. We perform a long-wavelength approximation to the Schrödinger equation underlying the TB Hamiltonian. It consists of expressing the spatial part of the wave function as the product of a fast-varying part times a slow-varying part. Within this approximation the wave function can be written as

$$\Psi_\alpha(\boldsymbol{R}_\alpha) \propto e^{i\boldsymbol{k}\cdot\boldsymbol{R}_\alpha} F_\alpha(\boldsymbol{R}_\alpha), \quad (11)$$

where $\alpha \in \{\text{A},\text{B},\text{H}\}$ and $\boldsymbol{R}_\alpha$ is the lattice site coordinate. We substitute this wave function into the Schrödinger equation and expand the slow-varying part as

$$F_\alpha(\boldsymbol{R}_{\alpha'} \pm \boldsymbol{d}_j) \simeq F_\alpha(\boldsymbol{R}_{\alpha'}) \pm \boldsymbol{d}_j \cdot \boldsymbol{\nabla}_{\boldsymbol{r}} F_\alpha(\boldsymbol{r})|_{r=R_{\alpha'}} + O(|\boldsymbol{d}|^2).$$

Collecting all terms we are left with

$$\tilde{\mathcal{H}} = v_{\rm F}\boldsymbol{\Sigma}\cdot\boldsymbol{p}, \quad (12)$$

where $v_{\rm F} = 2\ell_0 t$ is the Fermi velocity and $\boldsymbol{p} = (p_x, p_y, 0) = -i\hbar(\partial_x, \partial_y, 0)$. Here the pseudospin matrices are defined as

$$\Sigma_x = \begin{pmatrix} 0 & 1 & 0 \\ 1 & 0 & 0 \\ 0 & 0 & 0 \end{pmatrix}, \quad \Sigma_y = \begin{pmatrix} 0 & 0 & 0 \\ 0 & 0 & 1 \\ 0 & 1 & 0 \end{pmatrix}, \quad \Sigma_z = \begin{pmatrix} 0 & 0 & -i \\ 0 & 0 & 0 \\ i & 0 & 0 \end{pmatrix}. \quad (13)$$

These matrices fulfill the algebra of the angular momentum $[\Sigma_i, \Sigma_j] = i\epsilon_{ijk}\Sigma_k$ and form a three-dimensional representation of SU(2). However, contrary to the Pauli matrices, they do not form a Clifford algebra, that is, $\{\Sigma_i, \Sigma_j\} \neq 2\delta_{i,j}\mathbb{I}_3$. Therefore, while Eq. (12) describes electrons with a linear energy spectrum, it does not represent a Dirac Hamiltonian. By introducing a rotation operator around the z axis defined by $\mathcal{D}_z(\phi) = \exp(-i\Sigma_z\phi)$, a generic state $|\alpha\rangle$ is transformed into itself by $\mathcal{D}_z(2\pi)|\alpha\rangle \to |\alpha\rangle$, implying that the pseudospin $\boldsymbol{\Sigma}$ describes an integer spin $S = 1$.

A. Spin-orbit interaction

Within the long wavelength approximation we can also express the intrinsic SOI introduced in the previous section. This term reads

$$\tilde{\mathcal{H}}_{\rm SO} = \Delta_{\rm SO}\Sigma_z \otimes \sigma_z, \quad (14)$$

where $\Delta_{\rm SO}$ is the effective spin-orbit coupling strength and σ_z is a Pauli matrix. The energy spectrum can be computed in this regime and reads

$$\tilde{\varepsilon}_0^{(\rm SO)} = 0, \quad (15a)$$

$$\tilde{\varepsilon}_\pm^{(\rm SO)} = \pm\sqrt{v_{\rm F}^2|\boldsymbol{k}|^2 + \Delta_{\rm SO}^2}. \quad (15b)$$

This is twofold degenerate, with degeneracy corresponding to spin-up and spin-down.

B. Landau levels in a uniform magnetic field

The long-wavelength approximation also allows us to compute the Landau levels that arise in the presence of the uniform magnetic field. The system Hamiltonian reads

$$\tilde{\mathcal{H}}_B = v_{\rm F}\,\boldsymbol{\Sigma}\cdot\left(\boldsymbol{p} - \frac{e}{c}\boldsymbol{A}\right), \quad (16)$$

where $\mathbf{A}$ is the vector potential associated with the magnetic field $\boldsymbol{B} = (\boldsymbol{\nabla}\times\boldsymbol{A})$ perpendicular to the lattice plane.

We solve the Schrödinger equation in the Landau gauge with $\mathbf{A} = (-By, 0, 0)$. Furthermore, we make the Ansatz $\Psi = \psi(y)\exp(ikx)$. Introducing a k-dependent shift in the y coordinate $\sqrt{B}\xi = By + k$ we are left to solve a system of coupled linear differential equations

$$\xi\,\psi_{\rm H}(\xi) = \tilde{\varepsilon}\psi_{\rm A}(\xi), \quad (17a)$$

$$\xi\,\psi_{\rm A}(\xi) - i\,\psi_{\rm B}'(\xi) = \tilde{\varepsilon}\psi_{\rm H}(\xi), \quad (17b)$$

$$-i\,\psi_{\rm H}'(\xi) = \tilde{\varepsilon}\psi_{\rm B}(\xi) \quad (17c)$$

for the three components of $\psi(\xi)$. Here $\varepsilon = E/(\hbar v_F\sqrt{B})$ is the rescaled eigenenergy. The Landau levels at nonzero energy are given by

$$\psi_{\pm,\mathfrak{n}}(\xi) = \begin{pmatrix} (\sqrt{\mathfrak{n}}\phi_{\mathfrak{n}-1} + \sqrt{\mathfrak{n}+1}\phi_{\mathfrak{n}+1})/\sqrt{2} \\ \pm\sqrt{2\mathfrak{n}+1}\phi_{\mathfrak{n}} \\ -i(\sqrt{\mathfrak{n}}\phi_{\mathfrak{n}-1} - \sqrt{\mathfrak{n}+1}\phi_{\mathfrak{n}+1})/\sqrt{2} \end{pmatrix} \quad (18)$$

with corresponding eigenvalues $\tilde{\varepsilon}_{\pm,\mathfrak{n}} = \pm\sqrt{2\mathfrak{n}+1}$ and $\mathfrak{n}$ integer. Here the $\phi_{\mathfrak{n}}$ for $\mathfrak{n} \geqslant 0$ are the eigenfunctions of the one-dimensional harmonic oscillator,

$$\phi_{\mathfrak{n}}(\xi) = \frac{1}{\sqrt{2^{\mathfrak{n}}\pi^{1/2}\mathfrak{n}!}} h_{\mathfrak{n}}(\xi) e^{-\xi^2/2}, \quad (19)$$

where $h_{\mathfrak{n}}$ denotes the Hermite polynomial of order $\mathfrak{n}$, while we define $\phi_{-1} \equiv 0$. In addition to the eigenfunctions (18) there are two different types of solutions at energy $\tilde{\varepsilon}_{0,\mathfrak{n}} = 0$. The first of these is related to the flat band at zero magnetic field (1a) and reads

$$\psi_{0,\mathfrak{n}}(\xi) = \frac{1}{\sqrt{2}} \begin{pmatrix} \sqrt{\mathfrak{n}+1}\phi_{\mathfrak{n}-1} - \sqrt{\mathfrak{n}}\phi_{\mathfrak{n}+1} \\ 0 \\ -\mathrm{i}(\sqrt{\mathfrak{n}+1}\phi_{\mathfrak{n}-1} + \sqrt{\mathfrak{n}}\phi_{\mathfrak{n}+1}) \end{pmatrix}, \quad (20)$$

where $\mathfrak{n} > 0$. The second type of zero-energy Landau level is given by

$$\psi_0^{(0)}(\xi) = \frac{1}{\sqrt{2}} \begin{pmatrix} \phi_0 \\ 0 \\ i\phi_0 \end{pmatrix}. \quad (21)$$

Note that $\psi_0^{(0)}(\xi)$ is not a generalization of (20) to the case $\mathfrak{n} = 0$.

C. Spectrum with magnetic field and spin-orbit interaction

Now we turn to the effects of finite SOI on the Landau levels obtained above. The energies $\tilde{\varepsilon}_{\alpha,\sigma,\mathfrak{n}}$ (with $\alpha = \{0,\pm\}$ and $\sigma = \{\uparrow, \downarrow\}$) of the Landau levels are the three solutions of

$$\frac{\sqrt{\mathfrak{n}}}{\tilde{\varepsilon}_{\alpha,\sigma,\mathfrak{n}} - \sigma\Delta_{\mathrm{SO}}} + \frac{\sqrt{\mathfrak{n}+1}}{\tilde{\varepsilon}_{\alpha,\sigma,\mathfrak{n}} + \sigma\Delta_{\mathrm{SO}}} = \tilde{\varepsilon}_{\alpha,\sigma,\mathfrak{n}}. \quad (22)$$

The corresponding wave functions read

$$\psi_{\alpha,\sigma,\mathfrak{n}} = \frac{\sqrt{\mathfrak{n}}}{\tilde{\varepsilon}_{\alpha,\sigma,\mathfrak{n}} - \sigma\Delta_{\mathrm{SO}}}\phi_{\mathfrak{n}-1} \begin{pmatrix} 1 \\ 0 \\ -i \end{pmatrix} + \phi_{\mathfrak{n}} \begin{pmatrix} 0 \\ \sqrt{2} \\ 0 \end{pmatrix} + \frac{\sqrt{\mathfrak{n}+1}}{\tilde{\varepsilon}_{\alpha,\sigma,\mathfrak{n}} + \sigma\Delta_{\mathrm{SO}}}\phi_{\mathfrak{n}+1} \begin{pmatrix} 1 \\ 0 \\ i \end{pmatrix}. \quad (23)$$

In the case of weak SOI, that is, $\Delta_{\mathrm{SO}} \ll 1$, the Landau levels are given by

$$\tilde{\varepsilon}_{\pm,\sigma,\mathfrak{n}} = \pm\sqrt{2\mathfrak{n}+1} - \frac{\sigma\Delta_{\mathrm{SO}}}{4\mathfrak{n}+2} + O\left(\Delta_{\mathrm{SO}}^2\right) \quad (24)$$

$$\varepsilon_{0,\sigma,\mathfrak{n}} = \frac{\sigma\Delta_{\mathrm{SO}}}{2\mathfrak{n}+1} + O\left(\Delta_{\mathrm{SO}}^2\right). \quad (25)$$

Consequently, the main effect of finite SOI is to lift the spin degeneracy with a level separation that decreases with growing Landau level index $\mathfrak{n}$. Moreover, the former highly degenerate zero energy levels [cf. Eqs. (20) and (21)] are now split into a family of flat bands at energies $\varepsilon_{0,\sigma,\mathfrak{n}}$.

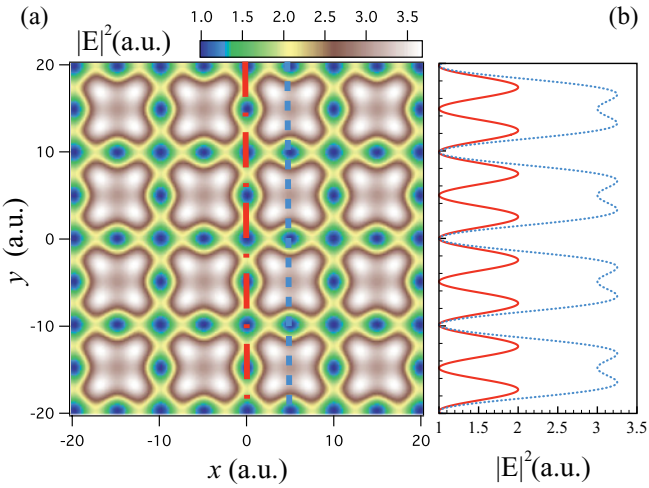

FIG. 6. (Color online) (a) Distribution of the laser field intensity for generating a Lieb lattice. (b) Two cuts through (a) corresponding to the B and H sites (red line) and A sites (blue dotted line).

IV. OPTICAL LATTICE REALIZATION

Reproducing the Lieb lattice with cold atoms trapped in optical lattices is a realistic and attracting goal [37], as it would pave the way for the exploration of flat band physics in a highly controllable environment. Experimentally the Lieb lattice can be realized as an optical lattice created by six counterpropagating pairs of laser beams. Four pairs are aligned along the x and y directions, two with wavelength $\lambda = \ell_0$ and two with wavelength $\lambda = \ell_0/2$. Finally, it requires two other laser pairs with a direction of $\pm 45^\circ$ with respect to the x axis. A detailed procedure leading to this choice of laser configuration has been discussed in Refs. [34,37]. The potential profile is given by the field

$$\begin{aligned} V_{\mathrm{OL}}(x,y) = {} & V_0[\sin^2(kx) + \sin^2(ky)] \\ & + V_1[\sin^2(2kx) + \sin^2(2ky)] \\ & + V_2\left[\cos^2\left(k\frac{x+y}{2}\right) + \cos^2\left(k\frac{x-y}{2}\right)\right], \end{aligned} \quad (26)$$

with $V_0 = V_1 = 2V_2$ and $k = \pi/\lambda$, which is depicted in Fig. 6. It is apparent that the hopping probability between A and B sites is exponentially small compared to the hopping probability between neighboring H and A and B pairs.

A. Simulation of the U(1) synthetic gauge field and quantum Hall phases

Recently synthetic U(1) magnetic fields for cold neutral atoms have been proposed [43,50,63] and experimentally realized [53]. In such setups atoms reproduce the dynamics of charged particles subjected to a uniform magnetic field and can effectively show quantum Hall phases. Several methods can be used in order to simulate the Hofstadter model [54] with these systems. These methods are generally based on the fact that the Peierls phases can be engineered by external optical [43,63] or magnetic [21] fields. These electromagnetic

fields can indeed induce hopping between neighboring lattice sites when the latter host atoms in different internal states, say $|g\rangle$ and $|e\rangle$. More precisely, the external fields trigger (Raman) couplings between these internal states, resulting in a NN-hopping amplitude

$$t_{g,e}e^{i\theta(\boldsymbol{x}_g)} \propto \int w^*(\boldsymbol{x}-\boldsymbol{x}_e)\Omega_{g,e}w(\boldsymbol{x}-\boldsymbol{x}_g)d^3x, \qquad (27)$$

where the Rabi frequency $\Omega_{g,e}$ typically includes space-dependent phase factors and where we suppose the states $|g\rangle$ and $|e\rangle$ to be trapped in neighboring sites [43,63]. Here the Peierls phase $\exp[i\theta(\boldsymbol{x}_g)]$ is directly related to the coupling laser's wave vector.

The gauge field (2), which leads to the Peierls phase (3), can be readily engineered in an optical lattice experiment by exploiting these methods [43,63]. From Fig. 1 it is clear that the x-dependent assisted hopping involves nearest neighbors and occurs along the y direction only, that is, between B and H sites. In this sense the phases $\theta(m)=\pi\Phi m$ can be realized on the optical Lieb lattice by extending the methods envisaged for the standard square lattice (cf. Refs. [43,50,63]). In the Lieb lattice case one should trap two internal states alternatively along the y direction: the B sites (H sites) should host an atom in the internal state $|g\rangle$ ($|e\rangle$). Coupling these states with external fields should then induce hoppings of the form (27), resulting in the space-dependent Peierls phase (3). Note that for generating a magnetic flux Φ per plaquette, a double phase $\theta_{\square}=2\theta=2\pi\Phi m$ is required for the square lattice compared to the Lieb lattice.

In the previous sections we have discussed the existence of quantum Hall phases in a fermionic Lieb lattice subjected to a uniform magnetic field. In order to produce these phases in a cold-atom experiment, one should engineer a U(1) gauge field for *fermionic* atoms. As already discussed in Ref. [21], most of the schemes generating gauge fields for bosons would lead to high spontaneous emission rates for fermionic atoms. Therefore realizing (integer) quantum Hall states would require alternative methods [63,76,77]. Such a proposal was introduced in Ref. [21] and uses radio-frequency magnetic fields produced by a set of current-carrying wires. The latter are periodically spaced on an atom chip and drive transitions between several internal states of ^{6}Li fermionic atoms. These effective "Raman transitions" lead to assisted hopping (27) and can be tuned in order to produce the desired Peierls phases. In order to engineer the U(1) gauge field (2), one can simplify the method initially proposed in Ref. [21] [which leads to the creation of SU(2) gauge fields] and consider transitions between two internal states of ^{6}Li, for example, $|g_1\rangle=|F=1/2,m_F=1/2\rangle$ and $|e_1\rangle=|3/2,1/2\rangle$. We stress that this practical scheme can be directly generalized to the Lieb lattice in order to generate the phases $\theta(m)=\pi\Phi m$ accompanying the hopping between neighboring H and B sites.

B. Simulation of the SU(2) gauge field with neutral atoms

Here we describe a practical scheme to simulate the intrinsic SOI term in a fermionic Lieb lattice. This coupling is equivalent to a SU(2) gauge field and could therefore be engineered in a multicomponent atomic system through

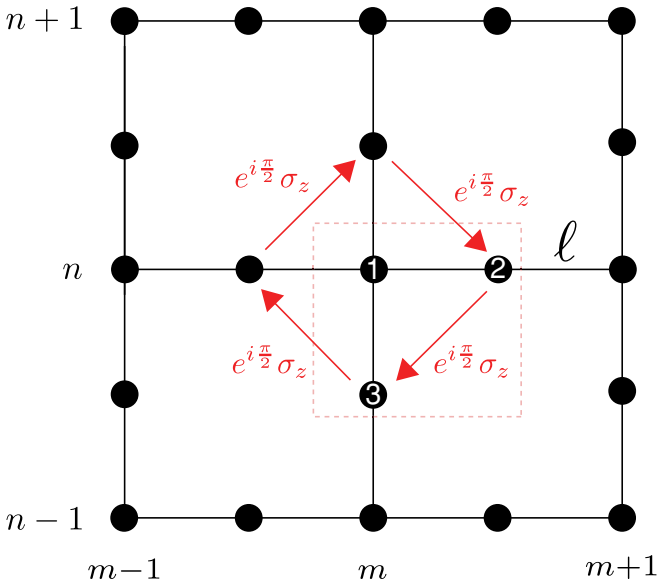

FIG. 7. (Color online) The Lieb lattice with the intrinsic spin-orbit coupling. This coupling is equivalent to a non-Abelian gauge field $\boldsymbol{A}$ leading to spin-dependent Peierls phases (as indicated by red arrows).

state-dependent Peierls phases (cf. Fig. 7). Our proposal is based on the observation that the spin-dependent NNN hoppings are equivalent to NN hoppings defined on the square sublattice formed by the A and B sites only [40] [cf. Fig. 8(a)]. Consequently, generating the SOI reduces to the simple problem of engineering the Peierls phases $e^{i\pi/2\sigma_z}$ on a *rotated* square lattice, which we now label using the notations $\tilde{m}$ and $\tilde{n}$ [cf. Fig. 8(b)]. Obviously the subtlety relies in the orientation of these phases: the phases are positive for a particle hopping, respectively, clockwise and anticlockwise in neighboring plaquettes [cf. Fig. 8(a)]. Note that this configuration reminds the structure produced by a staggered magnetic field with fluxes $\pm\Phi$ for each spin component [cf. Fig. 8(b)]. We note that in order to reproduce such a staggered field one can simply exploit the fact that the hopping induced by Raman transitions between the internal states g and e is such that $(te^{i\theta(x_g)})_{e,g}=(te^{i\theta(x_g)})^*_{g,e}$ [63].

Let us now describe a feasible and concrete scheme to synthesize the SOI term (6) in a cold-atom experiment. Our proposal requires four states $e_{1,2}$ and $g_{1,2}$ and external fields producing Raman transitions in both the $\tilde{x}$ and $\tilde{y}$ directions [cf. Figs. 8(a)–8(d)]. Such states can be chosen as being four internal states $|F,m_F\rangle$ of ^{6}Li, for example, $|g_1\rangle=|1/2,1/2\rangle$, $|g_2\rangle=|3/2,-1/2\rangle$, $|e_1\rangle=|3/2,1/2\rangle$, and $|e_2\rangle=|1/2,-1/2\rangle$ [21]. First, one needs to trap these states in state-dependent lattices [21,61,63] along the $\tilde{x}$ and $\tilde{y}$ directions [cf. Figs. 8(c) and 8(d)]. Then external fields should drive Raman transitions between these states, with the corresponding Rabi frequencies

$$\begin{aligned}\Omega^{\tilde{x}}_{g_1,e_1}&=\Omega^{\tilde{x}}_1, & \Omega^{\tilde{x}}_{g_2,e_2}&=\Omega^{\tilde{x}}_2,\\ \Omega^{\tilde{y}}_{e_1,g_1}&=\Omega^{\tilde{y}}_1, & \Omega^{\tilde{y}}_{e_2,g_2}&=\Omega^{\tilde{y}}_2,\end{aligned} \qquad (28)$$

as indicated by arrows in Figs. 8(c) and 8(d). At this point we emphasize that the Rabi frequencies are controlled by the

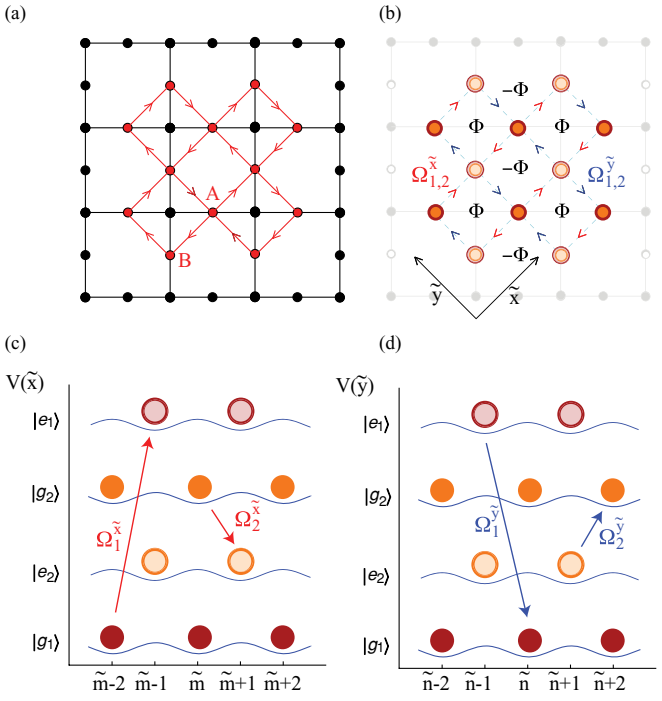

FIG. 8. (Color online) (a) The Lieb lattice with the intrinsic spin-orbit coupling. The Peierls phases (red arrows) are defined on the square sublattice formed by the A and B sites. (b) Laser assisted hoppings (arrows), associated couplings, and synthetic fluxes felt by the up-spin component. Four states $e_{1,2}$ and $g_{1,2}$ are trapped in state-dependent potentials and are represented by filled or empty orange or red disks (cf. figures below). (c) and (d) State-dependent potentials and couplings along the $\tilde{x}$ and $\tilde{y}$ directions. Here the potentials $V(\tilde{x})$, $V(\tilde{y})$ have different strength in order to control the hopping along the $\tilde{x}$ and $\tilde{y}$ directions individually.

coupling fields and that they are chosen to be different for transitions driven along the $\tilde{x}$ and $\tilde{y}$ directions [i.e., requiring state-dependent potentials $V(\tilde{x})$, $V(\tilde{y})$ with different strength]. Note that these Rabi frequencies typically contain phase factors depending on the coupling lasers wave vectors [43]. Moreover, the Rabi frequencies associated with the opposite transitions are simply given by $\Omega^{\tilde{\mu}}_{e_j,g_j} = (\Omega^{\tilde{\mu}}_{g_j,e_j})^*$, where $\tilde{\mu} = \tilde{x},\tilde{y}$. Therefore the hopping amplitudes along a given direction are accompanied by Peierls phases with alternating signs [63]. This is similar to a staggered magnetic field for each spin component, with fluxes $\pm\Phi$ [as illustrated in Fig. 8(b)] .

Now the SOI term (6) requires a specific configuration of these Rabi frequencies. The associated SU(2) gauge field is proportional to σ_z, which is simply achieved by imposing the constraint $\Omega^{\tilde{\mu}}_1 = (\Omega^{\tilde{\mu}}_2)^*$ (i.e., the coupling lasers should be characterized by opposite wave vectors). Besides, the desired gauge field is associated to constant Peierls phases [that is, $\exp(\pm i\pi/2)$], which further requires that the Rabi frequencies do not depend on the variables $\tilde{x},\tilde{y}$ and also obey the relation $\Omega^{\tilde{x}}_{1,2} = \Omega^{\tilde{y}}_{1,2}$ [or equally $\Omega^{\tilde{x}}_{g_j,e_j} = (\Omega^{\tilde{y}}_{g_j,e_j})^*$, using the definitions (28)].

We stress that this concrete scheme leads to the SOI studied in the previous sections and that it should open a QSH gap in an atomic setup. In order to observe the QSH phases induced by such a synthetic SOI in a cold-atom experiment, these nontrivial Peierls phases need to be engineered in a fermionic lattice. Again one can consider the atom-chip proposal of Ref. [21]: different sets of wires, aligned along $\tilde{x}$ and $\tilde{y}$, should trap the states e_j and g_j alternatively in both directions [as illustrated in Figs. 8(c) and 8(d)]. Additional "Raman wires" should then trigger RF transitions and couple the states, producing the induced hopping and associated phases described above. Another possibility would be to apply the superlattice methods of Refs. [63,76,77] to the Lieb lattice. Once the gauge field is synthesized, this setup needs to be superimposed with a state-independent Lieb lattice yielding the desired total Hamiltonian $\mathcal{H} = \mathcal{H}_0 + \mathcal{H}_{\rm SO}$.

Finally, we note that the scheme presented in this section could be simplified in order to reproduce the Abelian Haldane model on the Lieb lattice [6,17]. In this case only two internal states g and e would be needed, instead of four. A realization of the Haldane model on the Lieb lattice would lead to integer quantum Hall states [17].

C. DETECTION

The TB Hamiltonian and its long-wavelength approximation are valid for a Lieb lattice populated by single-component fermionic atoms, for example, ^{40}K or ^{6}Li. In this case the atomic collisions are negligible at low temperature [36]. From the experimental point of view, time-of-flight imaging via light absorption [78] can be used in order to detect the presence of massless fermions. The harmonic trap potential $V(\mathbf{r}) = m\omega^2\mathbf{r}^2/2$ confining the fermionic cold-atom gas is ramped down slowly enough for the atoms to stay adiabatically in the lowest band while their quasimomentum is approximatively conserved. Under these conditions free fermions expand with ballistic motion and, from the measured absorption images, it is possible [79,80] to reconstruct the initial reciprocal-space density profile of the trapped gas. Then the local density approximation (LDA) is typically well satisfied and the local chemical potential can be assumed to vary with the radial coordinate as $\mu(\mathbf{r}) = \mu_0 - V(\mathbf{r})$, where μ_0 is the chemical potential at the center of the trap. For a system of cold atoms at temperature T, the atomic density in the bulk is uniquely determined by the chemical potential

$$\rho(\mu) = \frac{1}{\mathcal{S}_0}\sum_\alpha \int f(\mathbf{k},\alpha,\mu)\, d\mathbf{k}\,. \tag{29}$$

Here $\mathcal{S}_0$ is the area of the first Brillouin zone of the Lieb lattice, and $f(\mathbf{k},\alpha,\mu) = (\exp\{[E_\alpha(\mathbf{k}) - \mu]/k_{\rm B}T\} + 1)^{-1}$ is the Fermi distribution function, where $E_\alpha(\mathbf{k})$ is the energy spectrum of the Lieb lattice [cf. Eq. (1)]. Figure 9(a) shows the atomic density ρ for the bulk as a function of the chemical potential μ. The contribution from the highly degenerate flat band (1a) manifests itself at $\mu = 0$ as a sharp jump in the atomic density. This feature is specific to lattices presenting flat bands [39]. For small finite μ we note that ρ evolves proportional to μ^2, which reflects the linear dispersion of massless fermions near the band center as well as particle-hole symmetry. On the contrary, for values of μ close to the maximum or minimum of the energy band, that is, far away from the band center (where

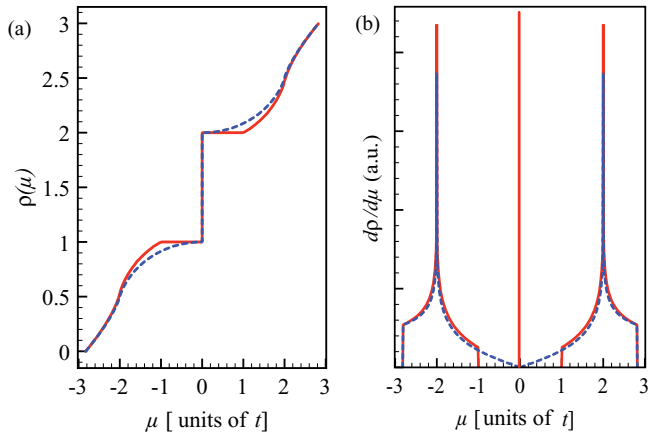

FIG. 9. (Color online) (a) Atomic density as a function of the chemical potential. (b) Density of states as a function of the chemical potential. The full line corresponds to $\Delta_{SO} = 0.25t$ and the dashed line to $\Delta_{SO} = 0$.

the long wavelength approximation can no longer be applied), ρ varies proportional to μ. When we consider a finite value of the SOI, a finite gap appears in the energy spectrum. This coincides with the horizontal segments in Fig. 9(a). Moreover, we can observe that the atomic density in proximity of the SOI gap is not anymore a quadratic function of the chemical potential but is behaving linearly. This is a signature of the mass term introduced by the finite SOI. In Fig. 9(b) we report the density of states (DOS) for two values of Δ_{SO}. Note the gap opening for $\Delta_{SO} \neq 0$ and the existence of two robust van Hove singularities at $\mu = \pm 2$. For a given confining potential $V(r)$, the density profile $\rho(r)$ can be obtained from Fig. 9(a) through the LDA. Therefore the SOI plateaus and van Hove singularities could be directly observed through *in situ* density measurements [63].

Let us stress the great similarity between the density and DOS obtained here for the Lieb lattice and those reported in Ref. [39] concerning the $\mathcal{T}_3$ lattice. However, these two lattices differ in their topological order since the SOI opens a *trivial* insulating gap in the $\mathcal{T}_3$ lattice [22]. This fundamental difference can be emphasized by computing the density profile $\rho(\mu)$ for the realistic finite-size system: in this case, gapless edge states contribute to the Lieb lattice atomic density and slightly tilt the SO plateaus. Note that this important effect, which is the direct signature of the topological phase, could only be observed for sufficiently small lattices (in which case the number of edge states is not totally negligible compared to the number of bulk states).

Finally, the methods for detecting topological properties, such as quantized Hall conductivity [79] and chiral edge states [20,21,40,81] have been discussed recently and could be easily generalized to our Lieb lattice setup. In this context an important issue is the stabilization of the edge states in the presence of a confining potential: these current-carrying states should be stabilized by sharp boundaries [20] or by designed interfaces induced by hopping anisotropy [21]. We finally note that robust quantization properties such as quantum Hall and quantum spin Hall phases rely on the existence of bulk energy gaps in the single-particle energy spectrum and further requires that the Fermi energy lies exactly inside such gaps (i.e., $\Delta E_F \sim 0.1t$).

V. SUMMARY

We have investigated the fermionic properties of a face-centered square (Lieb) lattice. This peculiar system is characterized by the presence of a single Dirac cone at the center of the first Brillouin zone and a flat energy band at half-filling. In particular we focused on the modification of this exquisite energy spectrum in the presence of an external magnetic field and a next-nearest-neighbor spin-orbit interaction. In the former case we have shown the opening of multiple gaps due to the occurrence of Landau levels which leads to the formation of two Hofstadter butterflies separated by the robust flat band at zero energy. We have characterized the topological nature of these gaps by investigating the IQHE. Inside the two Hofstadter butterflies, the Hall conductivity is quantized and each gap is characterized either by positive or negative values. Importantly, we find that the energy gaps separating the two butterflies have a trivial topological nature as they are characterized by zero Hall conductivity. This fact is a direct consequence of the flat band's trivial order. In the case of the spin-orbit interaction we have shown the opening of two symmetric gaps around the flat band. These are characterized by a nontrivial Z_2 topological phase leading to the quantum spin Hall effect. We have demonstrated the existence of helical edge states for an abstract cylindrical system, as well as for the more realistic finite lattice.

We have further investigated the Lieb lattice presenting a long-wavelength approximation for the system Hamiltonian around the single Dirac cone. We have shown that the Hamiltonian can be expressed in a relativistic form, similarly to the honeycomb lattice case, which is characterized by a set of pseudospin matrices of size 3×3. These matrices fulfill the commutation relation of an angular momentum and describe a spin-1 particle. Within the same approximation we have demonstrated that the spin-orbit interaction simply results in a mass term within the quasirelativistic Hamiltonian. Furthermore, we have inspected the properties of the Landau levels. In addition to the dispersion relation ruled by the square root of the Landau level index (as in the case of the honeycomb lattice) we have shown that there are two competing Landau levels at zero energy which are related to the lattice topology and to the symmetry class of the Hamiltonian operator.

This system and its associated properties could be engineered using fermionic cold atoms placed in an optical lattice resembling the Lieb lattice topology. We have proposed a method for implementing Abelian and non-Abelian synthetic gauge fields in order to simulate the presence of an external magnetic field and a next-nearest-neighbor spin-orbit interaction term. We have further shown that these synthetic fields trigger the opening of energy gaps while preserving the robust flat band at half-filling, properties which can be directly deduced from atomic density measurements. In particular, we emphasized that the Lieb lattice is very well suited to reproduce the intrinsic spin-orbit term introduced in Ref. [7], which in this case can be simply decomposed into nearest-neighbor hoppings on a square sublattice.

ACKNOWLEDGMENTS

N.G. thanks the F.R.S-F.N.R.S (Belgium) for financial support. D.B. is supported by the Excellence Initiative of the German Federal and State Governments. The authors thank A. Bermudez, N. Navon, Z. Lan, C. Weeks, M. Franz, P. Ohberg, F. Mei, I. Spielman, J. Dalibard, and F. Gerbier for useful discussions.

[1] K. von Klitzing, Rev. Mod. Phys. **58**, 519 (1986).
[2] D. J. Thouless, M. Kohmoto, M. P. Nightingale, and M. den Nijs, Phys. Rev. Lett. **49**, 405 (1982).
[3] M. Kohmoto, Ann. Phys. **160**, 343 (1985).
[4] Y. Hatsugai, Phys. Rev. B **48**, 11851 (1993).
[5] X.-L. Qi, Y.-S. Wu, and S.-C. Zhang, Phys. Rev. B **74**, 045125 (2006).
[6] F. D. M. Haldane, Phys. Rev. Lett. **61**, 2015 (1988).
[7] C. L. Kane and E. J. Mele, Phys. Rev. Lett. **95**, 146802 (2005).
[8] C. L. Kane and E. J. Mele, Phys. Rev. Lett. **95**, 226801 (2005).
[9] C. L. Kane and E. J. Mele, Science **314**, 1692 (2006).
[10] B. A. Bernevig and S.-C. Zhang, Phys. Rev. Lett. **96**, 106802 (2006).
[11] B. A. Bernevig, T. L. Hughes, and S.-C. Zhang, Science **314**, 1757 (2006).
[12] X.-L. Qi, T. L. Hughes, and S.-C. Zhang, Phys. Rev. B **78**, 195424 (2008).
[13] J. E. Avron, L. Sadun, J. Segert, and B. Simon, Phys. Rev. Lett. **61**, 1329 (1988).
[14] D. N. Sheng, Z. Y. Weng, L. Sheng, and F. D. M. Haldane, Phys. Rev. Lett. **97**, 036808 (2006).
[15] T. Fukui and Y. Hatsugai, Phys. Rev. B **75**, 121403(R) (2007).
[16] H.- M. Guo and M. Franz, Phys. Rev. B **80**, 113102 (2009).
[17] G. Liu, S. L. Zhu, S. Jiang, F. Sun, and W. M. Liu, Phys. Rev. A **82**, 053605 (2010).
[18] C. Weeks and M. Franz, Phys. Rev. B **82**, 085310 (2010).
[19] A. Ruegg, J. Wen, and G. A. Fiete, Phys. Rev. B **81**, 205115 (2010).
[20] T. D. Stanescu, V. Galitski and S. Das Sarma, Phys. Rev. A **82**, 013608 (2010).
[21] N. Goldman, I. Satija, P. Nikolic, A. Bermudez, M. A. Martin-Delgado, M. Lewenstein, and I. B. Spielman, Phys. Rev. Lett. **105**, 255302 (2010).
[22] D. Bercioux, N. Goldman, and D. F. Urban, Phys. Rev. A **83**, 023609 (2011).
[23] K. Sun, H. Yao, E. Fradkin, and S. A. Kivelson, Phys. Rev. Lett. **103**, 046811 (2009).
[24] H.- M. Guo and M. Franz, Phys. Rev. Lett. **103**, 206805 (2009).
[25] L. Fu, C. L. Kane, and E. J. Mele, Phys. Rev. Lett. **98**, 106803 (2007).
[26] M. Kargarian and G. A. Fiete, Phys. Rev. B **82**, 085106 (2010).
[27] H. Tasaki, Eur. Phys. J. B **64**, 365 (2008).
[28] E. H. Lieb, Phys. Rev. Lett. **62**, 1201 (1989).
[29] A. Mielke, J. Phys. A **24**, L74 (1991); **24**, 3311 (1991); **25**, 4335 (1992).
[30] D. L. Bergman, C. Wu, and L. Balents, Phys. Rev. B **78**, 125104 (2008).
[31] D. Green, L. Santos, and C. Chamon, Phys. Rev. B **82**, 075104 (2010).
[32] J. Vidal, R. Mosseri, and B. Douçot, Phys. Rev. Lett. **81**, 5888 (1998); J. Vidal, P. Butaud, B. Douçot, and R. Mosseri, Phys. Rev. B **64**, 155306 (2001); D. Bercioux, M. Governale, V. Cataudella, and V. M. Ramaglia, Phys. Rev. Lett. **93**, 056802 (2004); Phys. Rev. B **72**, 075305 (2005).
[33] E. Dagotto, E. Fradkin, and A. Moreo, Phys. Lett. B **172**, 383 (1986).
[34] R. Shen, L. B. Shao, B. Wang, and D. Y. Xing, Phys. Rev. B **81**, 041410(R) (2010).
[35] M. Lewenstein, A. Sanpera, V. Ahufinger, B. Damski, A. Sen (De), and U. Sen, Adv. Phys. **56**, 243 (2007).
[36] I. Bloch, J. Dalibard, and W. Zwerger, Rev. Mod. Phys. **80**, 885 (2008).
[37] V. Apaja, M. Hyrkäs, and M. Manninen, Phys. Rev. A **82**, 041402 (2010).
[38] G. Grynberg, B. Lounis, P. Verkerk, J.-Y. Courtois, and C. Salomon, Phys. Rev. Lett. **70**, 2249 (1993).
[39] D. Bercioux, D. F. Urban, H. Grabert, and W. Häusler, Phys. Rev. A **80**, 063603 (2009).
[40] X.-J. Liu, X. Liu, C. Wu, and J. Sinova, Phys. Rev. A **81**, 033622 (2010).
[41] Y.-J. Lin, R. L. Compton, A. R. Perry, W. D. Phillips, J. V. Porto, and I. B. Spielman, Phys. Rev. Lett. **102**, 130401 (2009).
[42] I. B. Spielman, Phys. Rev. A **79**, 063613 (2009).
[43] D. Jaksch and P. Zoller, New J. Phys. **5**, 56 (2003).
[44] T.-L. Ho and S. Zhang, e-print arXiv:1007.0650.
[45] G. Juzeliunas, J. Ruseckas, and J. Dalibard, Phys. Rev. A **81**, 053403 (2010).
[46] Y.-J. Lin, K. Jimenez-Garcia, and I. B. Spielman, Nature (London) **471**, 83 (2011)
[47] Z. Wang, X.-L. Qi, and S.-C. Zhang, New J. Phys. **12**, 065007 (2010).
[48] T. D. Stanescu, B. Anderson, and V. Galitski, Phys. Rev. A **78**, 023616 (2008).
[49] G. Juzeliunas, P. Ohberg, J. Ruseckas, and A. Klein, Phys. Rev. A **71**, 053614 (2005).
[50] J. Dalibard *et al.*, e-print arXiv:1008.5378v1.
[51] J. Ruostekoski, G. V. Dunne, and J. Javanainen, Phys. Rev. Lett. **88**, 180401 (2002).
[52] Y.-J. Lin, R. L. Compton, K. Jiménez-García, W. D. Phillips, J. V. Porto, and I. B. Spielman, Nature Phys. (2011).
[53] Y.-J. Lin *et al.*, Nature (London) **462**, 628 (2009).
[54] D. Hofstadter, Phys. Rev. B **14**, 2239 (1976).
[55] N. Goldman, A. Kubasiak, P. Gaspard, and M. Lewenstein, Phys. Rev. A **79**, 023624 (2009).
[56] A. S. Sørensen, E. Demler, and M. D. Lukin, Phys. Rev. Lett. **94**, 086803 (2005).
[57] M. Merkl, F. E. Zimmer, G. Juzeliunas, and P. Ohberg, Europhys. Lett. **83**, 54002 (2008).
[58] N. Goldman, A. Kubasiak, A. Bermudez, P. Gaspard, M. Lewenstein, and M. A. Martin-Delgado, Phys. Rev. Lett. **103**, 035301 (2009).
[59] Lih-King Lim, C. Morais Smith, and A. Hemmerich, Phys. Rev. Lett. **100**, 130402 (2008).

[60] K. J. Günter, M. Cheneau, T. Yefsah, S. P. Rath, and J. Dalibard, Phys. Rev. A **79**, 011604(R) (2009).
[61] K. Osterloh, M. Baig, L. Santos, P. Zoller, and M. Lewenstein, Phys. Rev. Lett. **95**, 010403 (2005).
[62] J. Ruseckas, G. Juzeliunas, P. Öhberg, and M. Fleischhauer, Phys. Rev. Lett. **95**, 010404 (2005).
[63] F. Gerbier and J. Dalibard, New J. Phys. **12**, 033007 (2010).
[64] C. Wang, C. Gao, C.-M. Jian, and H. Zhai, Phys. Rev. Lett. **105**, 160403 (2010).
[65] S.-L. Zhu, H. Fu, C.-J. Wu, S.-C. Zhang, and L.-M. Duan, Phys. Rev. Lett. **97**, 240401 (2006).
[66] E. Tang, J.-W. Mei, and X.-G. Wen, e-print arXiv:1012.2930; K. Sun, Z. Gu, H. Katsura, and S. Das Sarma, e-print arXiv:1012.5864.
[67] Note that while the energy spectrum was derived in Ref. [66], Fig. 3 significantly extends these previous results by showing the *phase diagram* describing the IQHE, which is encoded via the different coloring of the energy gaps.
[68] H. Aoki, M. Ando, and H. Matsumura, Phys. Rev. B **54**, 17296(R) (1996).
[69] M. Kohmoto, Phys. Rev. B **39**, 11943 (1989).
[70] Y. Hasegawa, Y. Hatsugai, M. Kohmoto, and G. Montambaux, Phys. Rev. B **41**, 9174 (1990).
[71] M. Kohmoto, J. Phys. Soc. Jpn. **61**, 2645 (1992).
[72] T. Fukui, Y. Hatsugai, and H. Suzuki, J. Phys. Soc. Jpn. **74**, 1674 (2005).
[73] Y. Hatsugai, T. Fukui, and H. Aoki, Phys. Rev. B **74**, 205414 (2006).
[74] The relation between $\Delta\sigma_{xy}$, the number of Weyl points, and the existence of a flat band has been recently explored by Z. Lan *et al.*, e-print arXiv:1102.5283.
[75] H. Min, J. E. Hill, N. A. Sinitsyn, B. R. Sahu, L. Kleinman, and A. H. MacDonald, Phys. Rev. B **74**, 165310 (2006).
[76] A. Bermudez, L. Mazza, M. Rizzi, N. Goldman, M. Lewenstein, and M. A. Martin-Delgado, Phys. Rev. Lett. **105**, 190404 (2010).
[77] L. Mazza, M. Rizzi, M. Lewenstein, and J. I. Cirac, Phys. Rev. A **82**, 043629 (2010).
[78] M. Köhl, H. Moritz, T. Stöferle, K. Günter, and T. Esslinger, Phys. Rev. Lett. **94**, 080403 (2005).
[79] R. O. Umucalilar, H. Zhai, and M. Ö. Oktel, Phys. Rev. Lett. **100**, 070402 (2008).
[80] T. L. Ho and C. V. Ciobanu, Phys. Rev. Lett. **85**, 4648 (2000).
[81] V. W. Scarola and S. Das Sarma, Phys. Rev. Lett. **98**, 210403 (2007).